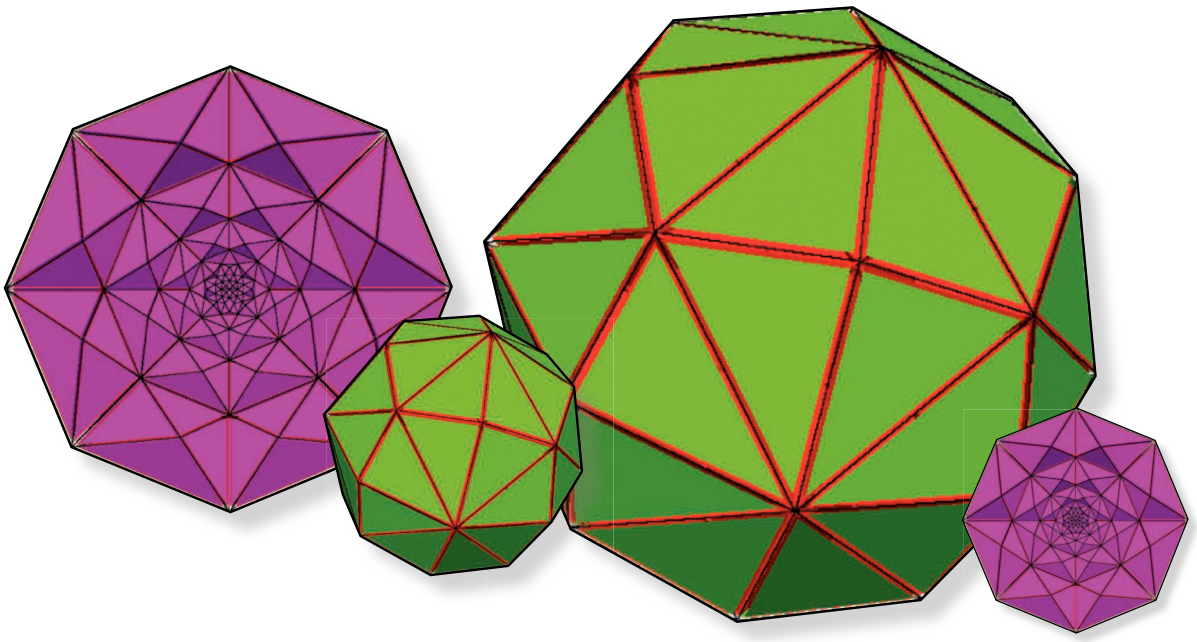

THIS ARTICLE OUTLINES HOW modern first-principle calculations can adequately address the need for ever-higher levels of numerical accuracy and high performance in large-scale electronic structure simulations as well as pioneer the fundamental study of quantum many-body effects in a large number of emerging nanomaterials.

ADVANCES IN FIRST-PRINCIPLE CALCULATIONS

The technology for electronic devices has been on a rapidly rising trajectory since the 1960s. The main factor in this development has been the ability to fabricate ever-smaller silicon CMOS devices ("Moore's law"), with today's device sizes in the nanometer range. The ability to control electronic materials and understand their properties has been a driving force for technological breakthroughs. The emergence of new nanoscale materials and devices, whose operating principles rely entirely on quantum effects, necessitates a

From Fundamental First-Principle Calculations to Nanoengineering Applications

A review of the NESSIE project.

JAMES KESTYN AND ERIC POLIZZI

Digital Object Identifier 10.1109/MNANO.2020.3024387
Date of current version: 13 October 2020

1942-7808/20©2020IEEE

fundamental and comprehensive understanding of the nanoscale physics of systems.

First-principle calculations offer a unique approach to study materials that start directly from the mathematical equations describing the physical laws and do not require any empirical parameters aside from fundamental constants. They are known as *electronic structure calculations* when applied to the configuration of electrons in a molecule or solid, which determine most of the physical properties of matter through chemical bonding.

The fundamental laws governing physics have been known since the beginning of the 20th century with the development of quantum mechanics. The difficulty, then, does not lie in formulating the problem but actually solving it. Atom-by-atom, large-scale, first-principle calculations have become critical for supplementing the experimental investigations and obtaining detailed electronic structure properties and reliable characterizations of emerging nanomaterials. These simulations are essential to assist the everyday work of numerous engineers and scientists and can universally impact a wide range of disciplines (engineering, physics, chemistry, and biology) that span the technological fields of computing, sensing, and energy.

In spite of the enormous progress that has been made in the last few decades, the room for improvement in first-principle calculations is still significant. Traditional numerical and modeling techniques are, indeed, largely inadequate to cope with the new generation of challenges encountered in large-scale nanoengineering applications, including systems with many thousands of atoms. Atomistic simulations must adapt to leverage the current needs in scalability by capitalizing on the massively parallel capabilities of modern high-performance computing (HPC) platforms.

Additionally, well-established public or commercial software packages were originally intended to investigate the basic electronic structure properties of materials using ground-state calculations. They possess only limited capabilities for performing excited-state calculations that can efficiently model and predict quantum many-body effects in emerging nanomaterials. The ability to capture these fundamental nanophysics effects is increasingly important for exploring and prototyping new, revolutionary, functional materials in nanotechnology.

There is an urgent need in nanoengineering for new, quantum-based, transformative solutions that will play a key role in future electronics, including plasmonics, phononics, and excitonics. Future breakthroughs could enable disruptive technologies to compete directly with CMOS or be integrated into existing systems to increase throughput and decrease power dissipation. To this end, new 1D and 2D nanostructures [e.g., graphene, carbon nanotubes (CNTs), molybdenum disulfide (MoS_2), and layered transition metal dichalcogenides] have been the center of large research efforts, with first-principle atomistic simulations playing a significant role. Plasmonic devices, which rely on collective many-body effects, have also shown promise as high-frequency analog sensors to be used in biomedical applications and telecommunications.

This article presents the entire computational process needed to bring fundamental first-principle calculations up to the level where they can significantly impact innovations in nanoengineering. As depicted in Figure 1, modern first-principle calculations must be capable of 1) achieving both accuracy and scalability, 2) allowing for the study of emerging many-body functionality, and 3) fully taking advantage of recent advances in algorithm development for HPC.

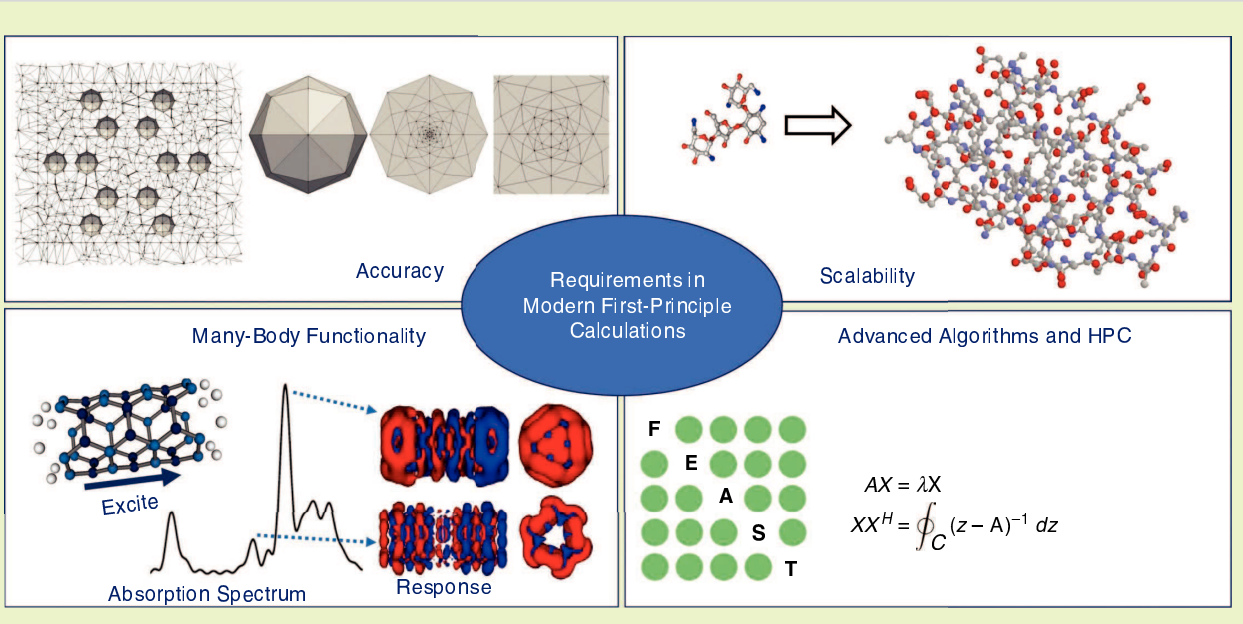

FIGURE 1 The requirements in modern first-principle calculations at a glance.

In spite of the enormous progress that has been made in the last few decades, the room for improvement in first-principle calculations is still significant.

FIRST-PRINCIPLE MODELING: FROM PHYSICS TO ALGORITHMS

The field of first-principle modeling can be broadly separated into three categories:

- Physical models reduce the complexity of the full many-body solution while keeping much of the important physics. The choice of a physical model is often motivated by the objectives of the simulations.
- Discretization and mathematical models can transform physical equations into the language of linear algebra.
- Computing and numerical algorithms are used to solve the resulting problems.

To improve on current software implementation by fully capitalizing on modern HPC computing platforms, it is essential to revisit all of the various stages of the electronic structure modeling process, which are briefly summarized in the following sections.

PHYSICAL MODELING

A direct numerical treatment of a full many-body Schrödinger equation leads to a deceptively simple linear eigenvalue problem, which is well known to be intractable because of its exponentially growing dimension with the number of particles. This limitation has historically motivated the need for lower levels of sophistication in the description of the electronic structure using a single-electron picture approximation, where the dimension of the Hamiltonian operator ends up scaling linearly with the number of electrons. First-principle electronic structure calculations are usually performed within the single-electron picture [1], [2] using either quantum chemistry (i.e., post-Hartree–Fock) methods or, as an alternative to wave function-based methods, density functional theory (DFT) associated with the Kohn–Sham equations [3], [4].

Although DFT does not allow for systematic accuracy as traditional quantum chemistry techniques would, it is the method of choice when dealing with moderate-sized systems containing more than a handful of atoms. DFT has been widely used in computational material science for decades, since it provides (in principle) an exact method for calculating the ground-state density and energy of a system of interacting electrons using a nonlinear, single-electron, Schrödinger-like equation associated with exchange-correlation (XC) functionals.

In practice, the reliability of DFT depends on the numerical approximations used for the XC terms that range from the simplest local density approximation (LDA) or the generalized gradient approximation (GGA) to more advanced (hybrid) schemes, which are still the subject of active research efforts [5]–[8]. Solutions of the DFT/Kohn–Sham problem are routinely used in the calculations of many ground-state properties, including total energy and ionization potential, crystal-atomic structure, ionic forces, vibrational frequencies, and phonon band structure via perturbation theory.

Although DFT cannot fundamentally provide information on excited states and many-body properties, the Kohn–Sham eigenvectors are often needed by more advanced techniques: e.g., either Green's function-based [9] (e.g., GW, Bethe–Salpeter) or time-dependent, density-based [i.e., time-dependent density functional theory (TDDFT) [10], [11]] approaches. The pros and cons of these approaches are discussed in [12].

TDDFT, proposed by Runge and Gross [13], continues to gain popularity as one of the most numerically affordable many-body techniques capable of providing fairly accurate results. TDDFT has been successfully applied to calculate many physical observables of the time-dependent Hamiltonian, such as excitation energies and complex permittivities as well as nonlinear phenomena. It is often used to obtain the absorption spectra of complex molecular systems. While the design of advanced time-dependent XC functionals is still a challenging task [14], adiabatic LDA (ALDA) for TDDFT has been found to perform extremely well on a wide variety of systems by capturing many nanoscopic effects (such as plasmonic effects) that, in turn, can be quantitatively compared with the experimental data.

TDDFT calculations can be performed in the frequency or real-time domains. The real-time TDDFT technique is a relatively recent approach introduced by Yabana and Bertsch in [15] and [16], and it has become an important focus of TDDFT research activities. It has notably been integrated into the software packages Octopus [17], [18], NWChem [19], and GPAW [20] for the study of molecular systems. In essence, spectroscopic information can be obtained using the standard formalism of dipole time response from weak short-polarized impulses in any given direction of the system; this requires all of the occupied single-electron wave functions to be propagated (nonlinearly) in time.

The imaginary part of the dipole's Fourier transform provides the dipole strength function. The absorption spectrum is then obtained along with the expected "true many-body" excited energy levels. In contrast to the numerical models derived from the TDDFT linear response theory in the frequency domain [10], [21]–[23], the real-time TDDFT approach is better suited for achieving linear parallel scalability, and it can also address any form of nonlinear responses, including ion dynamics [24].

MATHEMATICAL MODELING AND DISCRETIZATION

Although first-principle calculations have provided a practical (i.e., numerical tractable) path for solving the electronic

structure problem, they have also introduced new numerical challenges. Within the single-electron picture, the resulting eigenvalue problem becomes fully nonlinear since the Hamiltonian operator depends on all of the occupied eigenfunctions [i.e., $H(\{\psi\})\psi = E\psi$].

In practice, this nonlinear eigenvector problem is commonly addressed using direct minimization schemes or self-consistent field (SCF) methods wherein a series of linear eigenvalue problems (i.e., $H\psi = E\psi$) needs to be solved iteratively until convergence. Computing the electron density at a given iteration step becomes one of the most time-consuming and challenging parts of the DFT electronic structure calculations. Successfully reaching convergence by performing SCF iterations is of paramount importance to first-principle electronic structure calculation software. Real-time TDDFT also comes with its own set of mathematical and numerical challenges for performing the time propagation; these are discussed further in the "First-Principle Calculations Using NESSIE" section.

To perform the numerical calculations, the mathematical models need first to be discretized by expanding the wave functions over a set of basis functions. One can identify three main discretization techniques that have been widely used over the past four decades by both the quantum chemistry and solid-state physics communities [1]:

- the linear combination of atomic orbitals (LCAO) (along with the dominant use of Gaussian local basis sets)
- the plane wave expansion scheme
- real-space mesh techniques [25]–[37] (also loosely called *numerical grids*) based on the finite difference, finite element (FEM), spectral element, or wavelets methods.

Each of these approaches has pros and cons.

- Plane waves have traditionally been used within the solid-state physics community because their natural periodic nature can be easily applied to crystal structures. However, this can be cumbersome when dealing with finite systems where the computational domain must be made much larger than the molecular size to ensure that interactions due to periodicity are negligible. Additionally, they often make use of pseudopotentials to mimic the effects of core electrons, which do not directly participate in chemical bonding and would otherwise necessitate a very large number of plane waves due to their high-frequency variations.
- LCAO benefits from a large collection of local basis sets that has been improved and refined throughout the years by the quantum chemistry community to obtain a high level of accuracy in simulations. However, LCAO bases may suffer from numerical truncation errors of finite expansions, and the solutions cannot be universally and systematically improved toward convergence.
- Real-space mesh techniques provide a natural way of quantifying atomic information by employing universal local mathematical approximations. They can easily handle the treatment of various boundary conditions, such as Dirichlet (for the confined directions), periodic, or absorbing (for transport simulations). Similar to plane wave schemes, however, the high level of refinement needed to capture the core electrons may be problematic.

To perform the numerical calculations, the mathematical models need first to be discretized by expanding the wave functions over a set of basis functions.

In all cases, the level of approximation in the discretization stage is bounded by the capabilities of the numerical algorithms for solving the resulting system matrices. In modern nanoelectronic applications, one aims at fully utilizing the power of modern HPC architectures to tackle large-scale, finite systems by exploiting parallelism at multiple levels. In this context, real-space mesh techniques offer the most significant advantages. They produce very sparse matrices that can take advantage of recent advances in linear scaling $O(N)$ methods and domain-decomposition (DD) techniques.

COMPUTING

Much of the progress in this field is directly tied to advancements in algorithmic research allowing larger and more complex systems to be simulated. Within the SCF-DFT procedure, computing the electron density by solving the linear and symmetric eigenvalue problem at each iteration becomes the major computational challenge. The characterization of complex systems and the nanostructures of current technological interests requires the repeated computations of many tens of thousands of eigenvectors for eigenvalue systems that can have sizes in the tens of millions.

It is important to mention that Green's function-based formalism can alternatively be used to directly compute the electron density (using efficient evaluations of the diagonal elements of the Green's function along a complex contour, e.g., [38]–[40]). However, this method gives rise to difficulties in algorithmic complexity [i.e., $O(N^2)$ for 3D systems], parallel scalability, and accuracy. In that regard, it is difficult to bypass the wave function formalism, and progress in large-scale electronic structure calculations can then be tied together with advances in numerical algorithms for addressing the eigenvalue problem in particular.

The traditional methods for solving the eigenvalue problem (including the Arnoldi or Lanczos methods as well

as other Davidson–Jacobi techniques [41], [42]) and related packages [43] are largely unable to cope with these challenges. In particular, they suffer from the orthogonalization of a very large basis when many eigenpairs are computed. In this case, a divide-and-conquer approach that can compute wanted eigenpairs by parts becomes mandatory, since "windows" or "slices" of the spectrum can be computed independently of one another, and orthogonalization between eigenvectors in different slices is no longer necessary.

These issues have motivated the development of a new family of eigensolvers based on contour integration techniques [44]–[47], such as the FEAST eigensolver [48], [49]. FEAST is an optimal accelerated-subspace, iterative technique for computing interior eigenpairs, making use of a rational filter to approximate the spectral projector [50]. FEAST can be applied for solving both the standard and generalized forms of Hermitian or non-Hermitian problems [72]. Once a given search interval is selected, FEAST's main computational task consists of solving a set of independent linear systems along a complex contour.

Not only does the FEAST algorithm feature some remarkable and robust convergence properties [50], [51], it can exploit natural parallelism at three different levels (L1, L2, or L3):

- *L1*: Search intervals can be treated separately (no overlap).
- *L2*: Linear systems can be solved independently across the quadrature nodes of the complex contour.
- *L3*: Each complex linear system with multiple right-hand sides can be solved in parallel.

Parallel resources can be placed at all three levels simultaneously to achieve scalability and optimal use of the computing platform.

FIRST-PRINCIPLE CALCULATIONS USING NESSIE

A first-principle simulation software must be capable of addressing all of the modern challenges summarized in Figure 1. One of the major goals in modern first-principle calculations is to develop numerical algorithms and simulation software for electronic structures that can scale the system size to thousands of atoms without resorting to additional approximations beyond the DFT and TDDFT physical models. The target computing architecture is usually composed of thousands of processor cores and contains multiple hierarchical levels of parallelism.

The NESSIE project [52] is an electronic structure code that uses a real-space FEM discretization and DD to perform all-electron ground-state DFT and real-time excited-state TDDFT calculations. NESSIE gets its name from an FEM legacy code for quantum transport [53] that has evolved over time to include first-principle simulations. The code is written to take advantage of multilevel parallelisms to target systems containing many distributed-memory compute nodes. Custom numerical algorithms have been developed for the eigenvalue problems and linear systems representing the major linear algebra operations within the software.

NESSIE's capabilities can be separated into three main categories:

- accurate large-scale, full-core potential DFT calculations using real-space FEM discretization and DD
- TDDFT real-time propagation for efficient spectroscopic calculations, allowing the study of many-body effects
- massively parallel implementation on modern high-end computing platforms using state-of-the-art parallel algorithms/solvers.

The next sections present a step-by-step description of NESSIE's modeling framework applied to the benzene molecule as an example.

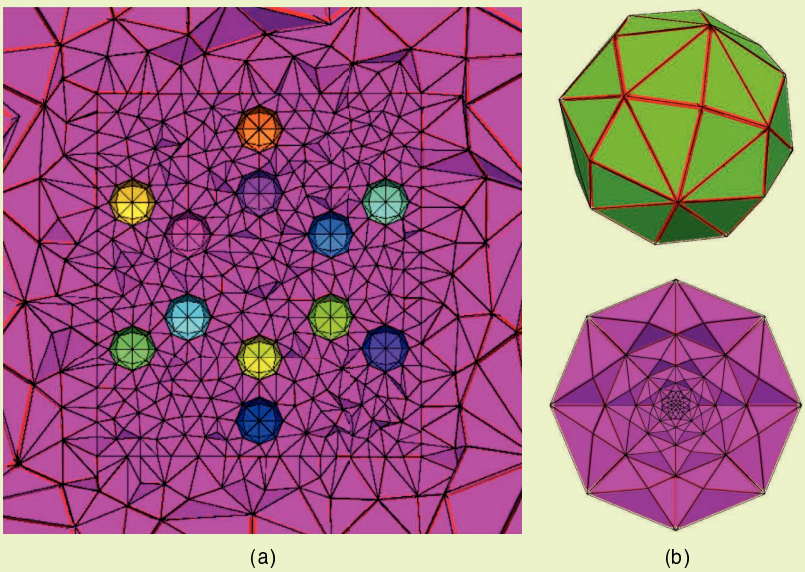

FIGURE 2 Using a muffin tin DD method, the whole simulation domain is separated into multiple atom-centered regions (i.e., muffins) and one large interstitial region. (a) A 2D section of local FEM discretization using a coarse interstitial mesh (represented only partially here) connecting all of the atoms of a benzene molecule. (b) A finer mesh for the atomic (muffin) regions suitable for capturing the highly localized core states around the nuclei.

AN ALL-ELECTRON HPC MUFFIN TIN FRAMEWORK

In NESSIE, the equations are discretized using FEM with quadratic (P2) or cubic (P3) order, along with a muffin tin DD technique. The latter was proposed as early as the 1930s [54] to specifically address a multicenter atomic system. The whole simulation domain is separated into multiple atom-centered regions (i.e., muffins) and one large interstitial region. Without any loss of generality, Figure 2 illustrates the essence of the muffin tin DD using FEM and applied to the benzene molecule.

The 3D finite-element muffin tin mesh can be built in two steps: 1) a 3D atom-centered mesh, which is highly refined around the nucleus to capture

the core states; and 2) a much coarser 3D interstitial mesh that connects all of the muffins (generated in NESSIE using Tetgen software [55], [56]). For the atom-centered mesh, which is common to all atoms of the same atomic number, it is convenient to use successive layers of polyhedral, similar to the ones proposed in [37]. This discretization provides both tetrahedra of good quality and an arbitrary level of refinement i.e., the distance between layers can be arbitrarily refined while approaching the nucleus (this is known as an *h-refinement* for FEM).

The muffin tin decomposition can bring flexibility in the discretization step (different basis sets can also be used independently to describe the different regions), can reduce the main computational efforts within the interstitial region alone, and should also guaranteed maximum linear parallel scalability performances. It is important to note that, independent of the type of atoms, the outer layer of the muffin is consistently providing the same (relatively small) number of connectivity nodes n_I with the interstitial mesh at the muffin edges (i.e., n_I = 98, or 218 nodes, respectively, using the quadratic P2 or cubic P3 FEM). Consequently, the size of the system matrix in the interstitial region stays independent of the size of the atom-centered regions, and the approach can then ideally deal with the full potential (all electrons).

Once the "Schrödinger" eigenvalue problem (i.e., $H\psi = E\psi$) is reformulated using DD strategies, the resulting (and still exact) problem now takes a nonlinear form in the interstitial region [i.e., $H_I(E)\psi_I = E\psi_I$, since the boundary conditions at the interfaces with the muffins are energy dependent]. As originally pointed out by Slater in 1937 while introducing the muffin tin augmented plane wave (APW) method, this nonlinear eigenvalue problem gives rise to an energy-dependent secular equation that cannot be handled by traditional eigenvalue algorithms.

Although solving such a nonlinear problem explicitly is not impossible [57], [58], it remains practically challenging, and it is still the subject of active research efforts [59], [60]. Therefore, the mainstream approaches to all-electron (i.e., full-potential) electronic structure calculations in the solid-state physics community have mostly relied on approximations, such as direct linearization techniques, which have been improved throughout the years [e.g., linear augmented plane wave (LAPW), linear muffin-tin orbitals (LMTO), and so on] [61]–[65]. Alternatively, linear eigenvalue problems can be obtained directly from pseudopotential approximation techniques [66]–[69] that eliminate the core states by introducing smooth but nonlocal potentials in muffin-like, atom-centered regions.

In NESSIE, an exact strategy has been introduced for performing all-electron electronic structure calculations within a parallel computing environment [70], [71]. The approach relies on the shift-and-invert capability of eigenvalue algorithms, such as FEAST, which leads to formulating well-defined linear systems. DD methods have been well studied and are a natural framework for addressing large, sparse linear systems generated from real-space meshes. They are often associated with the use of distributed-memory numerical algorithms to address the data distribution using the message passing interface (MPI) paradigm. Consequently, the solution of FEAST's linear systems can be fully parallelized using MPI since the muffin tin decomposition naturally allows each muffin to be factorized and solved independently.

When the muffin tin decomposition is applied to a given linear system, the resulting linear system in the interstitial domain (as well as the Schur complement) remains linear. The details of the muffin-DD strategy implementation have been provided in [70]. In essence, the muffin-DD linear solver operates in three stages:

1) The atoms are distributed throughout the MPI processors and factorized at a given energy pivot (i.e., the shift value provided by FEAST); the boundary conditions (as well as self-energy) are then derived at the interfaces of the muffins.
2) The resulting interstitial linear system (Schur complement) is solved in parallel.
3) Knowing the exact solution at the muffin interfaces, the solution within each muffin is retrieved in parallel.

In comparison with the linearization techniques discussed previously, the set of "pivot energies" used to evaluate the interstitial Hamiltonian system is now explicitly provided by the FEAST algorithm (i.e., they correspond to quadrature nodes in the complex plane), and it guarantees global convergence toward the correct solutions (i.e., no approximation is needed). Since the complexity of the interstitial system scales linearly with the number of atoms while including nonlocality only at the interfaces with the muffins, one can also demonstrate that this all-electron framework is (paradoxically) capable of better scalability performances than pseudopotential approaches on parallel architectures.

The FEAST solver has been recently significant upgraded to support the MPI–MPI–MPI distributed parallel programming model in version 4.0 [86] (where the last "MPI" refers to the linear system solves at L3). Furthermore, NESSIE can take advantage of the first two MPI levels of parallelism offered by FEAST assuming that the eigenvalue spectrum is distributed among the compute nodes. At L2, FEAST can naturally distribute all of the linear systems associated with a given search interval (typically fewer than 10). At L1, FEAST enables "spectrum slicing," where all of the intervals of interest are solved in parallel.

The use of spectrum slicing is essential to address a major bottleneck in large-scale DFT calculations concerning the computation and storage of the DFT wave functions. The storage requirement, in particular, keeps increasing linearly with the number of electrons in the nanostructures. Even with a simplified physical model, such as DFT, it becomes particularly difficult to scale the electronic structure problem for systems containing more than a few hundred electrons without the ability to perform spectrum slicing. This technique is illustrated for benzene in Figure 3, using three elliptical contours for FEAST, one that computes the core states and two others that compute half of the valence states. In larger systems, each contour often contains hundreds of eigenvalues.

DFT GROUND-STATE CALCULATIONS AND SCALABILITY

The DFT/Kohn–Sham problem can be expressed as

$$\left[-\frac{\hbar^2}{2m}\nabla^2 + v_{KS}[n](\mathbf{r})\right]\psi_i = E_i\psi_i,$$
$$\text{with} \quad n(\mathbf{r}) = 2\sum_{i=1}^{N_e} |\psi_i(\mathbf{r})|^2, \qquad (1)$$

where the Kohn–Sham potential, $v_{KS}[n] = v_H[n] + v_{XC}[n] + v_{\text{ext}}$, is composed of the Hartree potential v_H (the solution of the Poisson equation), the XC potential, and other external potentials v_{ext} including the ionic core potential. The N_e lowest occupied electronic states $\{\psi_i\}_{(i=1,\ldots,N_e)}$ are needed to compute the electron density (the factor 2 stands for the electron spin).

Formally, the system (1) forms a nonlinear eigenvector problem that is commonly addressed using an SCF method wherein a series of linear eigenvalue problems needs to be solved iteratively until convergence. The naive approach, which consists of updating the input electron density at each SCF iteration directly from the output electron density, results in large oscillations between SCF iterations. This approach is very unlikely to converge, as the initial guess for the density is usually far from the ground-state solution. Instead, traditional SCF methods employ successive approximation iterates of fixed-point mapping to generate the new input electron (as well as "mixing" techniques).

DFT CONVERGENCE

Using a mixing technique, two different electron densities are considered to construct the input density at the $(k+1)$th SCF iteration: the input density ρ_{in}^k used to construct the Kohn–Sham Hamiltonian and the output density ρ_{out}^k computed from the wave functions. With simple mixing, the input electron density for the next iteration can be computed as

$$\rho_{\text{in}}^{k+1} = (1-\beta)\rho_{\text{in}}^k + \beta\rho_{\text{out}}^k, \qquad (2)$$

where the parameter β is usually chosen as less than one-half. This, however, will converge very slowly. To increase the convergence rate, more sophisticated methods have been developed for solving this fixed-point problem.

Newton methods cannot be used in electronic structures since it is impractical to construct the Jacobian matrix. Other quasi-Newton methods were developed in the 1960s, notably by Anderson [73] and Broyden [74], that do not require the Jacobian or Hessian. These techniques were later refined in the 1980s in the context of SCF iteration by Pulay [75], [76] and have since been expanded upon [77]–[80]. They are also related to Krylov and generalized minimal residual methods [81]–[83]. For electronic structure calculations, these iterative techniques are usually referred to as *direct inversion of the iterative subspace methods*. The general idea is to build the input electron density as a linear combination of past densities. One can then construct the input mixing density,

$$\hat{\rho}_{\text{in}}^{k+1} = c_0\rho_{\text{in}}^0 + c_1\rho_{\text{in}}^1 + \cdots + c_k\rho_{\text{in}}^k, \qquad (3)$$

and the output mixing density,

$$\hat{\rho}_{\text{out}}^{k+1} = c_0\rho_{\text{out}}^0 + c_1\rho_{\text{out}}^1 + \cdots + c_k\rho_{\text{out}}^k, \qquad (4)$$

from the previous input and output densities. The input for the next iteration is chosen as a linear combination:

$$\rho_{\text{in}}^{k+1} = (1-\beta)\hat{\rho}_{\text{in}}^{k+1} + \beta\hat{\rho}_{\text{out}}^{k+1}, \qquad (5)$$

where β is, again, referred to as the *mixing parameter*. This approach can be truncated to keep the density subspace size small. The inclusion of more densities in the mixing subspace can result in better convergence, but it has diminishing returns. Keeping a history of 10 to 20 input and output densities seems to be more than sufficient. Better performance can be obtained by choosing a

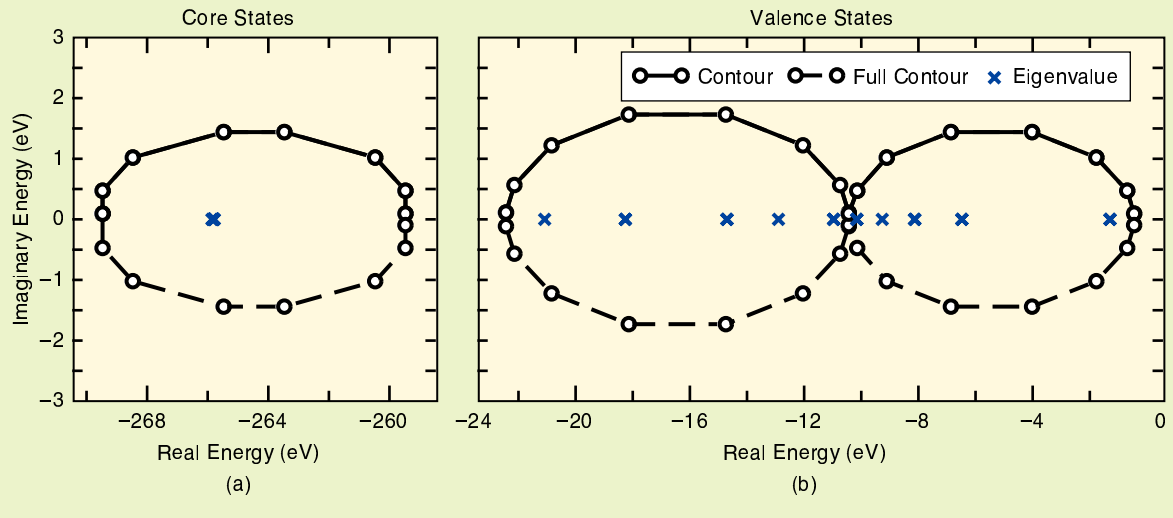

FIGURE 3 Splitting the full search interval into three separate contours for benzene. (a) The lowest energy contour captures the core states, while (b) the other two target valence electrons. Each half-contour has eight quadrature nodes, shown as circles. Symmetry allows the FEAST algorithm to perform computations only for the upper half of the contour (solving eight independent linear systems per interval).

larger value of β, but it may also result in instability. However, improvement in convergence can be obtained by progressively increasing the β parameter along the SCF iterations as the input and output densities become closer.

The coefficients $\{c_0,\ldots,c_k\}$ of (3) and (4) are the same for both the input and output mixing subspaces. They are computed by solving a $k\times k$ linear system with one right-hand side,

$$M_{k\times k}c_{k\times 1} = r_{k\times 1}, \tag{6}$$

where the ith element of r depends on the difference between the output and input densities of the current iteration k and a previous iteration i,

$$r_i = \int_\Omega \rho^k_{\text{out,in}} \times [\rho^k_{\text{out,in}} - \rho^i_{\text{out,in}}]\,d\Omega, \tag{7}$$

where $\rho^p_{\text{out,in}} = (\rho^p_{\text{out}} - \rho^p_{\text{in}})$, and each element M_{ij} of matrix M takes into account the densities at iterations i and j:

$$M_{ij} = \int_\Omega [\rho^k_{\text{out,in}} - \rho^i_{\text{out,in}}] \times \left[\rho^k_{\text{out,in}} - \rho^j_{\text{out,in}}\right] d\Omega. \tag{8}$$

In NESSIE, the mixing scheme can take advantage of one important feature of the FEAST eigensolver. As the density begins to converge, the previous eigenvector subspace solution can be used as a very good initial guess for solving the current eigenvalue problem. Since the eigenvalue convergence criteria are set to only slightly exceed the current SCF convergence, FEAST must perform only a single subspace iteration on average and, with parallelism, solve a single linear system per diagonalization.

The other major numerical operation in ground-state DFT is the computation of the Hartree potential—the potential corresponding to a classical charge distribution—through the solution to the Poisson equation. Once the Dirichlet boundary conditions have been determined at the edge of simulation domain, this amounts to solving a real symmetric-positive, definite linear system with one right-hand side. The Poisson equation, then, gives rise to a much less expensive linear system than the ones obtained with the eigenvalue computation. The computation of the boundary conditions for Poisson uses the integral form of the Poisson equation and scales as $O(N_s^2/p)$, where N_s is the number of surface nodes (which stays relatively small using a coarse FEM mesh far from the atomistic region), and p is the total number of MPI processes.

Selected DFT/LDA ground-state simulation results for benzene obtained using NESSIE and other all-electron first-principle software programs are reported in Table 1. The NESSIE results are in excellent agreement with those of the other approaches. In addition, a real-space mesh discretization, such as FEM, can easily be refined either by adding more local mesh nodes or by increasing the accuracy of the basis functions. Consequently, the numerical solutions can systematically converge toward the exact solutions at the level of the physical model (LDA in the example).

DFT SCALABILITY

In Table 1, the NESSIE FEM discretization leads to system matrices of size 2, 454 for the atom-centered mesh (i.e., a single muffin) using P2 or 8, 155 using P3. The interstitial size matrix varies from 20, 653 for P2 to 69, 305 for P3. These system matrices can effectively be handled in parallel using the muffin tin decomposition and spectrum slicing approach presented in Figures 2 and 3. For example, using only two search intervals (one for the core and one for the valence states; i.e., L1 = 2 in FEAST), eight contour points per interval (so eight linear systems in total; i.e., L2 = 8 in FEAST), a molecule like benzene with 12 atoms (i.e., L3 = 12 in FEAST) can effectively scale up to $2\times 8\times 12 = 192$ MPI processes on HPC platforms.

In general, the three levels of parallelism of FEAST can work together to minimize the time spent in all stages of the algorithm. L3 can be used to reduce the memory per node and to decrease the solution time of both the linear system factorization and solution. L2 has close-to-ideal scaling and, if fully utilized, can reduce the algorithmic complexity by solving a single complex linear system per FEAST iteration. L1, in turn, allows for the computation of a very large number of eigenvalues by subdividing the full search interval.

The simulation results obtained in [86] have demonstrated that NESSIE's muffin tin approach associated with the FEAST eigensolver is ideally suited for achieving both strong and weak scalability on high-end HPC platforms. Some results on weak scalability (i.e., the number of MPI processes increases proportionally with the number of atoms) are reported in Figure 4. These results outline, in particular, the efficiency of the muffin tin DD solver in comparison with other "black-box" sparse parallel direct solvers.

TDDFT EXCITED-STATE CALCULATIONS

In TDDFT theory, all of the occupied N_e ground-state wave function $\Psi = \{\psi_1, \psi_2, \ldots, \psi_{N_e}\}$ solutions of the Kohn–Sham system for the ground-state problem (1) are used as the initial

TABLE 1 **The DFT energy results for benzene (including the first core eigenvalue, the highest occupied molecular orbital level, and total energy) obtained using different all-electron first-principle software and basis functions, but the same LDA approach [85], to model the XC term.**

METHOD	ENERGY (eV)		
	E_1	E_{HOMO}	E_{tot}
NWChem 6–311 g* [19]	–266.35	–6.4	–6,262.27
NWChem cc-pvqz [19]	–266.41	–6.52	–6,263.65
P2-FEM [37]	–264.66	–6.54	–6,226.57
P3-FEM [37]	–266.38	–6.53	–6,262.57
P4-FEM [37]	–266.44	–6.53	–6,263.78
FHI-AIMS [37], [84]	–266.44	–6.53	–6,263.83
NESSIE P2-FEM	–266.39	–7.04	–6,244.45
NESSIE P3-FEM	–266.49	–6.55	–6,263.41

conditions for solving a time-dependent Schrödinger-type equation ($\forall i = 1, \ldots, N_e$):

$$\imath\hbar\frac{\partial}{\partial t}\psi_i(\mathbf{r},t) = \left[-\frac{\hbar^2}{2m}\nabla^2 + v_{KS}[n](\mathbf{r},t)\right]\psi_i(\mathbf{r},t), \quad \text{with} \quad n(\mathbf{r},t) = 2\sum_{i=1}^{N_e} |\psi_i(\mathbf{r},t)|^2, \quad (9)$$

where the electron density of the interacting system can then be obtained at any given time from the time-dependent Kohn–Sham wave functions. In principle, TDDFT can be used to calculate any time-dependent observable as a functional of the electron density. In (9), the Kohn–Sham potential becomes a function of the time-dependent density:

$$v_{KS}(n(\mathbf{r},t)) = v_{\text{ext}}(\mathbf{r},t) + v_H(n(\mathbf{r},t)) + v_{XC}(n(\mathbf{r},t)),$$

where it is common practice to consider a local dependency on time for the XC potential term v_{XC} (as well as the adiabatic approximation).

REAL-TIME PROPAGATION

Assuming a constant time step Δ_t, the integral form of (9) introduces the time-ordered evolution operator $\hat{U}(t+\Delta_t, t)$, such that

$$\Psi(t+\Delta t) = \hat{U}(t+\Delta_t, t)\,\Psi(t), \quad \text{with} \quad \hat{U}(t+\Delta_t, t) = \mathcal{T}\exp\left\{-\frac{\imath}{\hbar}\int_t^{t+\Delta_t} d\tau H(\tau)\right\}. \quad (10)$$

There exist a large number of efficient numerical methods for solving this real-time propagation problem [89], which can broadly be classified into two categories:

1) Partial differential equation-based techniques, such as the Crank–Nicolson (CN) scheme [90], can be used, where

$$\hat{U}(t+\Delta_t, t) = \left[1 + \frac{i}{2}\Delta_t H(t+\Delta_t/2)\right]^{-1} \times \left[1 - \frac{i}{2}\Delta_t H(t+\Delta_t/2)\right]. \quad (11)$$

This is an implicit scheme that requires solving a linear system at each time step.

2) Integral-based methods act directly on the evolution operator, such as the midpoint exponential rule, i.e.,

$$\hat{U}(t+\Delta_t, t) = \exp\{-\imath\Delta_t H(t+\Delta_t/2)\}. \quad (12)$$

This represents the starting point for splitting methods [91], Magnus expansion [92], or other spectral decompositions [93], [94].

If Δ_t is small enough, one can usually assume that $H(t+\Delta_t/2) \simeq H(t)$. Alternatively, corrector–predictor schemes can be used to evaluate the Hamiltonian at $(t+\Delta_t/2)$. The nonlinear nature of the time propagation arises from the Kohn–Sham v_{KS} potential that needs to be re-evaluated at each time step to form the new Hamiltonian. The Hartree potential v_H and exchange and correlation potential v_{XC} are both functionals of the electron density. The time-dependent Hartree potential is the solution of the Poisson equation, while the XC term can be computed with the time-instantaneous electron density (using the adiabatic approximation), and the same approximation used in the ground-state calculations (such as LDA or GGA).

The CN scheme for TDDFT is particularly effective within the NESSIE framework, since the linear system solved along the time steps in (11) can take

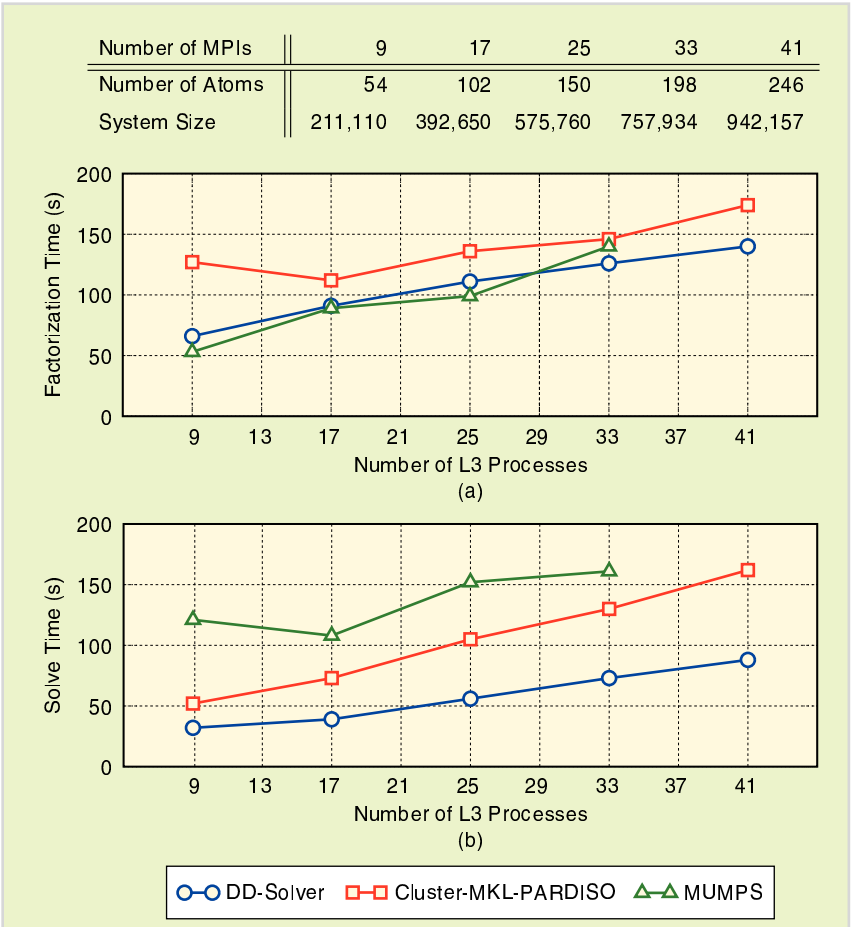

FIGURE 4 The L3 weak scaling of the (a) factorization and (b) solve stages for a single FEAST iteration using 16 contour points (L2 = 1 here) and 600 right-hand sides (i.e., a search interval with up to 600 states). The matrix size is increased proportionally with the number of MPI processes (using 12 cores per MPI of Haswell E5-2680v3—so 492 cores in total for the 246-atom systems). The results show that the muffin-DD solver outperforms both the MKL-Cluster-PARDISO [87] and MUMPs solvers [88]. The overall timings can be easily reduced by a factor 16 using L2 = 16 MPI parallelism (using 7,872 cores in total). Finally, the timings can be further improved by increasing the number of MPI processes for a fixed-atom-size system (strong scalability).

advantage of the highly scalable muffin tin real-space DD approach (Figure 2). As a result, the approach can be parallelized at two different MPI levels: 1) by propagating independent chunks of the occupied wavefunctions along Δ_t and 2) by solving the linear system in parallel.

Spectral-based schemes for the integral approach (12) are known to be robust and accurate, permitting larger time steps than the other usual integration schemes. They are, however, rarely used in practice for large-scale simulations since a direct diagonalization of the evolution operator (12) would require solving hundreds to thousands of eigenvalue problems along the time domain (i.e., one large-scale eigenvalue problem per time step). In addition to CN, NESSIE includes an efficient spectral-based approach that relies on the efficiency of the FEAST eigensolver [93].

First, good approximations of the exponential in (12) can be obtained with a partial spectral decomposition using an eigenvector subspace four to five times the number of propagated states ψ_j. Since the latter are low-energy states, this truncated spectral basis is typically sufficient to accurately expand the solutions. Second, FEAST can reuse the eigenvector subspace computed in the current time step as a very good initial guess for the next one. As a result, only one or two subspace iterations are usually sufficient to obtain convergence.

While the linear systems arising in CN need to be solved one after another along small time intervals, a parallel FEAST implementation permits the solution of a single linear system by larger time intervals. Although the FEAST linear system is notably more computationally demanding, i.e., including a lot of extended states, linear parallel scalability can still be naturally achieved using multiple search intervals and more parallel computing power.

It is worth mentioning that the same strategy would not be possible with the techniques used in TDDFT linear response theory in the frequency domain (e.g., using the Casida equation [10]), where the demand in extended states is even higher and represents the bottleneck of their cubic arithmetic complexity.

In general, the three levels of parallelism of FEAST can work together to minimize the time spent in all stages of the algorithm.

Consequently, if one can keep up with the demand in parallel computing power, direct diagonalizations for the real-time TDDFT formalism using FEAST become a viable high-performance alternative to other schemes, potentially capable of both higher scalability and better accuracy for obtaining linear and nonlinear responses.

DIPOLE–TIME RESPONSE

In principle, all time-dependent observables are functionals of the density; however, in practice, the functional form is rarely known. A very useful case of TDDFT is related to spectroscopy, where the absorption and emission spectra corresponding to electronic excitations can be derived directly from the induced dipole moment $d(t)$. The latter is related to the response of the system to an applied electric field E:

$$d(t) = \int_{-\infty}^{t} \alpha(t-t')\,E(t')\,dt', \quad (13)$$

where α is defined as the dynamic polarizability. In general, E and d are vectors quantities with x, y, and z components, and α is a tensor. In computational spectroscopy, one often considers the response of the system in a given direction μ (e.g., x, y, or z) associated with an excitation polarized in the same direction. The induced dipole moment in (13) can be calculated as a measure of how far the electron density $n(r, t)$ has moved away from its ground-state value n_0 along a given direction μ [17], [95], [96]:

$$d_\mu(t) = -q\int_\Omega (\mu - r_0)(n(r,t) - n_0(r))\,dr, \quad (14)$$

where r_0 stands for the molecular center of mass. As a result, for an isotropic material, it is possible to compute the dynamic polarizability by inverting (13). In the frequency domain (after the Fourier transform), the expression becomes

$$\alpha(\omega) = \frac{d(\omega)}{E(\omega)}. \quad (15)$$

In practice, it is necessary to introduce an artificial damping signal into the computed dipole moment before taking its Fourier transform:

$$d(\omega) = \int_0^T (d(t) \times e^{-\gamma t}) e^{i\omega t}\,dt, \quad (16)$$

where γ is a damping coefficient. This damping term is used to mimic the system relaxation effect since the TDDFT simulations presented here do not explicitly account for energy dissipation (i.e., a system would physically emit energy as photons and relax back to the ground state after being excited).

In time-dependent simulations, any external electric field $E(t)$ may be considered. It is common practice, however, to use either a step potential $u(t)$ or an impulse excitation $\delta(t)$, both along a given direction [16]. Table 2 presents the resulting expressions for the dynamic polarizability $\alpha(\omega)$ after Fourier transforms of these particular electric fields.

Finally, the imaginary part of the dynamic polarizability provides the photoabsorption cross section [97], which is related to the probability that a photon passing through the atomistic system is

TABLE 2 The polarizability for excitations in the form of an impulse potential and a step potential.

$E(t)$	$\alpha(\omega)$
$E_0 \times \delta(t)$	$-d(\omega)/E_0$
$E_0 \times u(t)$	$-i\omega \times d(\omega)/E_0$

E_0 stands for the amplitude of the electric field.

absorbed. A measure of the strength of this interaction (as well as the oscillator strength) can be computed from the polarizability as follows [98], [99]:

$$\sigma(\omega) = \frac{4\pi\omega}{c}\Im(\alpha(\omega)). \tag{17}$$

Once the oscillator strength (ω) is plotted as a function of the frequency ω (or, equivalently, the absorption energy), it provides the absorption spectrum of the system. As an example, Figure 5 shows the variations of the induced dipole moment for benzene obtained after three distinct impulse excitations polarized in the x, y, and z directions as well as the corresponding three absorption spectra.

RESONANCES AND RESPONSE DENSITY

The peaks in the absorption spectrum correspond to specific quantum many-body excitations (such as plasmon, band–band, and so on). The electron dynamics for a specific peak can be investigated further by computing and then visualizing the response density in 4D. Such simulations aim at providing more details on the electron dynamics of the particular resonances with relevant information about their nature.

The response density $\delta n(\omega, r)$ is the change in electron density due to an excitation at frequency ω (i.e., charge oscillations at ω). One possible way to visualize $\delta n(\omega, r)$ is by applying a sinusoidal excitation at a given frequency of interest, waiting for the induced dipole moment to reach a steady state where it oscillates at ω, and plotting the 4D data when the dipole reaches a maximum and a minimum [100]. Another more efficient

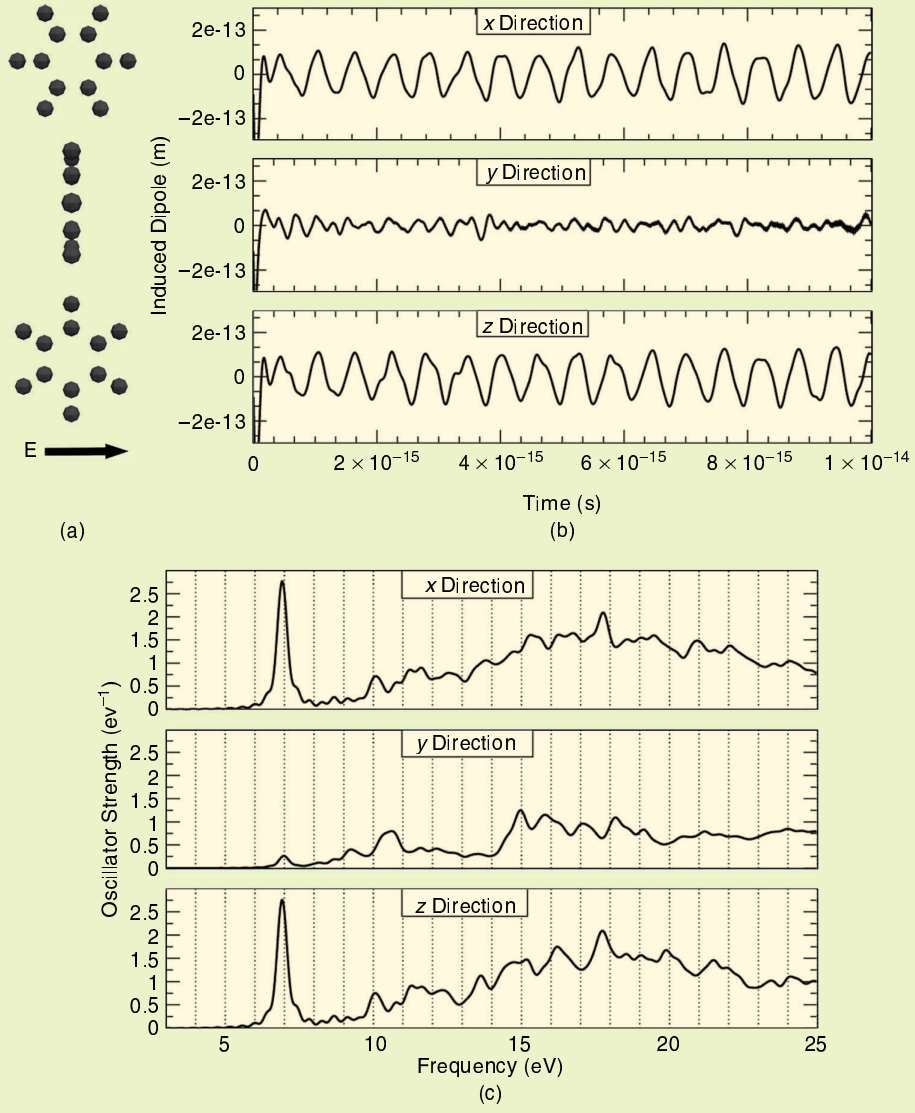

FIGURE 5 (a) The relative orientation of the benzene molecule if the applied electric field was polarized from left to right. (b) The induced dipole moment for benzene after an impulse excitation polarized in the x (top), y (middle), and z (bottom) directions (time steps of 5 attoseconds are used). (c) The corresponding absorption spectra.

approach consists of computing $\delta n(\omega, r)$ directly following the same procedure used for deriving the dipole moment in (14) and (16), which leads to

$$\delta n(r,\omega) = \int_0^T (n(r,t) - n_0(r))e^{-\gamma t}\, e^{i\omega t}\, dt. \quad (18)$$

In practice, there is no need to store all of the $n(r, t)$ functions, which would be prohibitive. Once the peaks/resonances of interests (i.e., $\{\omega_j\}$) have been identified in the absorption spectrum (for a given polarized excitation), one can proceed by running a new time-dependent TDDFT calculation to compute the response density $\delta n(r, \omega_j)$ (all frequency $\{\omega_j\}$ at once) using an on-the-fly Fourier transform of the time-varying electron density. The results from this approach are shown in Figure 6 for a few selected peaks in the absorption spectrum of benzene when the molecule is excited with an impulse electric field polarized in the z direction (as shown in Figure 5).

TDDFT ACCURACY AND RELIABILITY

The direction-independent absorption spectrum, which is computed as the average of the spectra in the x, y, and z directions, can be directly and quantitatively compared with the experimental data, if available. Figure 7 compares the experimental absorption spectra of various molecules with NESSIE's first-principle simulation results (obtained at $T = 0$K). In general, the TDDFT simulation results compare remarkably well with the experimental data for a large number of atomistic systems.

While the choice of the XC functional can significantly impact the reliability of the DFT ground-state results, a simple ALDA approximation for TDDFT appears to be sufficient for a wide variety of systems. Using NESSIE, it is also interesting to note that the choice of P2 versus P3 FEM basis functions has only a minimal impact on the accuracy of the absorption spectrum [71]. This is clearly not the case for DFT ground-state calculations as reported in Table 1, where good accuracy would require an appropriate level of refinement for FEM (using at least cubic P3 FEM). As a result, the real-time TDDFT framework appears to be resilient to some approximations (such as the choice of XC term or basis functions) as long as they are not too far off and stay consistent throughout the time propagation.

In addition to the opportunity to perform X-ray spectroscopy, there are many other advantages of considering a full real-space, all-electron treatment in simulations. In contrast to other approaches, a full-core, real-space potential offers numerical consistency while performing simulations in the time domain. Transferability issues are, indeed, likely to happen with the use of pseudopotentials that are generated for time-independent calculations or, in turn, with the use of an LCAO basis, which cannot offer the same reliability in capturing both the confined and extended states (although LCAO bases can be "augmented" in time-dependent simulations).

Comparisons between the NESSIE and LCAO approaches are reported in Table 3. Although NESSIE is using both a low level of real-space approximation (P2 FEM) and a rather simple XC term (LDA), the results compare relatively well with the experimental data. These results are actually, on average, much better than the ones obtained with the NWChem software.

The computing challenges end up being very similar between ground-state DFT and excited-state, real-time TDDFT calculations.

LARGE-SCALE, REAL-TIME TDDFT SIMULATIONS

The computing challenges end up being very similar between ground-state DFT and excited-state, real-time TDDFT calculations. There are only two main operations to consider: 1) solving a Hamiltonian linear system with multiple right-hand sides using, in particular, the muffin tin technique and 2) solving a linear system for the Poisson equation (using the local XC). For DFT, these two steps have to be repeated self-consistently until convergence, while, for TDDFT, they need to be repeated at each time step of the time propagation (using either a CN or a spectral decomposition scheme).

In comparison to other approaches, the muffin tin solver has demonstrated great efficiency in achieving strong and weak scalability [86] (see Figure 4). The scalability bottleneck of the muffin tin solver would eventually come from solving the interstitial Hamiltonian system in parallel using MPI (the Schur complement discussed in the "An All-Electron HPC Muffin Tin Framework" section). In practice, our strong and weak scalability results show that, up to 1,000 atoms (corresponding to an interstitial matrix with a size of ~1 million), this system can be efficiently solved using a standard

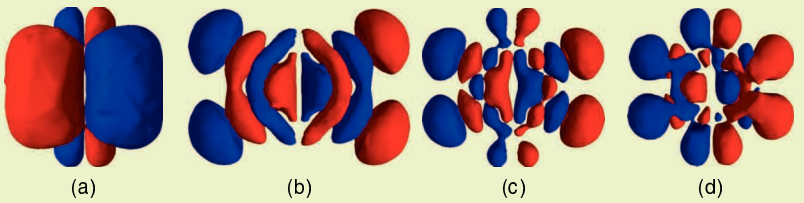

FIGURE 6 The 4D isosurface plots of the response electron density for four different peaks chosen from the absorption spectrum of z-polarized excited benzene (electric field going from left to right). Four frequency ω values are represented: (a) 6.91, (b) 10.04, (c) 13.61, and (d) 16.20 eV.

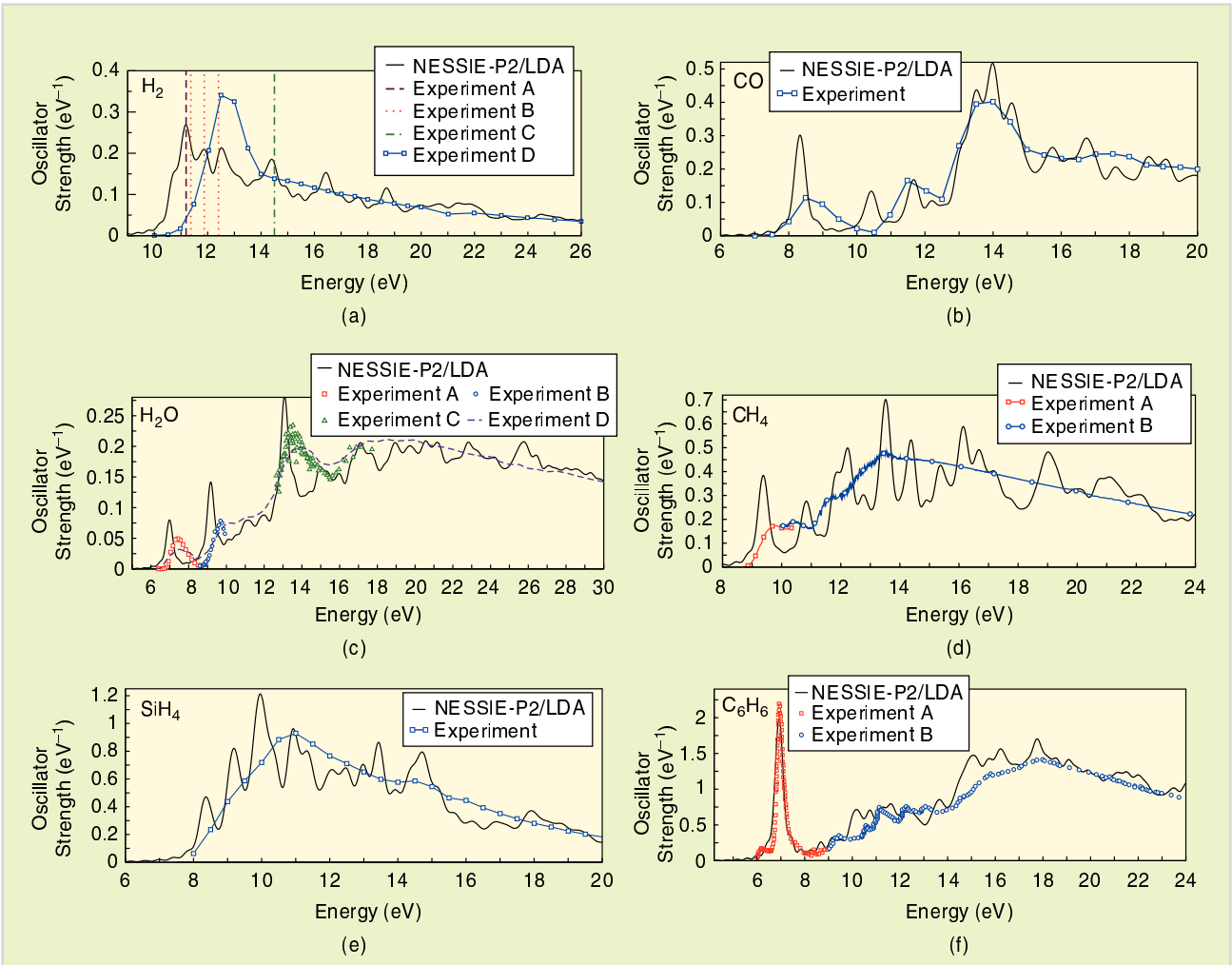

FIGURE 7 A comparison among the computed absorption spectra for various molecules using NESSIE (with ALDA and P2 FEM) and multiple sets of experimental values for (a) H_2 (experiments A [101], B [102], C [103], and D [104]), (b) CO [105], (c) H_2O (experiments A [106], B [107], C [108], and D [109]), (d) CH_4 (experiments A [110] and B [111]), (e) SiH_4 [112], (f) and C_6H_6 (experiments A [113] and B [114]).

TABLE 3 **A comparison of real-time TDDFT NESSIE and NWChem simulation results, with the experimental data for the lowest excitation energies (in eV), as reported in [115].**

METHOD	H_2	CH_4	CO	C_6H_6
NWChem-ccpvtz/LDA	12.31	10.29	8.28	7.1
NWChem-ccpvtz/B3LYP	12.90	10.75	8.55	7.18
NESSIE-P2/LDA	11.19	9.4	8.4	6.9
Experiment	11.19	9.70	8.55	6.9

NWChem uses the ccpvtz basis function and LDA or more advanced B3LYP XC functional.

direct "black-box" parallel sparse system solver (such as the cluster version of the Pardiso solver available in Intel's Math Kernel Library [87]). Reaching the milestone of 10,000 atoms and beyond is still the subject of active research efforts that investigate new directions in numerical linear algebra, such as the use of hybrid parallel solvers with customized low-communication preconditioners.

NANOPLASMONIC APPLICATIONS

Nanoplasmonics is a field that has grown rapidly in the last few years [116], [117], and it already offers numerous applications to electronics and photonics. In the visible and near-infrared (IR) range, nanoantennas [118] and nanoparticles have provided drastically enhanced coupling to electromagnetic waves [119], [120]. A 2008 comment in *Nature Nanotechnology* [118] stated, "Molecular components promise to revolutionize the electronics industry, but the vision of devices built from quantum wires and other nanostructures remains beyond present-day technology. Making such devices will require an extremely detailed knowledge of the properties of these components, such as the dynamics of charge carriers, electron spins, and various excitations, on nanometer-length scales and subpicosecond timescales at very high (up to THz [terahertz]) frequencies."

Reference [118] points out that single-wall CNT resonators would constitute a unique terahertz ultracompact circuit element, which might, for example, be used to control a terahertz oscillator source. Similar opportunities exist in the IR and visible ranges. One concludes that the discovery of new plasmonic materials is mandatory for the future expansion of the field of nanoplasmonics.

In [100], NESSIE was used to provide evidence of the plasmon resonances (collective electron excitations) in a number of representative short, 1D, finite carbon-based nanostructures using real-time TDDFT simulations. The simulated systems ranged from small molecules, such as C_2H_2, to various carbon nanostructures that are equivalent to 1D conductors with finite lengths, including carbon chains, narrow armchair and zigzag graphene nanoribbons [i.e., acenes and poly(p-phenylene)], and short CNTs.

The NESSIE all-electron TDDFT/ALDA model was able to accurately capture the bright components of the spectra, which account for the plasmonic excitation. The chief signature of 1D plasmons is a high-frequency excitation that is inversely proportional to the length of the conductor. In particular, it was shown that metallic 1D CNTs can be well described with the Tomonaga–Luttinger theory. The plasmon velocity is expected to reach an asymptotic value (up to three to five times the single-particle Fermi velocity) when the simulations are extended to tens of unit cells, such as very long CNTs, that become relevant for terahertz spectroscopy.

Since the reported preliminary work on short CNTs [100] (about five unit cells), NESSIE has been upgraded to simulate large-scale atomistic systems by taking advantage of new HPC techniques, such as the muffin-DD solver presented and discussed in the "An All-Electron HPC Muffin Tin Framework" section. This all-electron, real-space and real-time TDDFT framework is now capable of simulating very large structures (up to tens of unit cells for CNTs—from 100 atoms to a few thousand), leading to more relevant predicted data of the plasmonic effects for 1D systems. As an example, Table 4 summarizes the main NESSIE parameters and simulation results while considering increasingly longer (3,3)-CNTs. These results show that the position of the plasmon excitation peak (lowest excitation energy/frequency, i.e., E_p, f_p) keeps shifting with longer CNTs. The corresponding absorption spectra are provided in Figure 8.

In Table 4, the plasmon velocity is obtained with the reasonable assumption that the plasmon (collective electron cloud) must travel back and forth the full length L of the nanotube to complete a single oscillation (i.e., $v_p = 2Lf_p$). This is further supported by the 4D isosurface plots of the response density $\delta n(\omega, r)$ (18) in Figure 8, which have been calculated for the specific plasmon resonances. The plasmon velocity increases to 2.54 times the Fermi velocity ($\simeq 10^6$ m/s) for the 40 unit cells (3,3)-CNT, and it is expected to level off if we keep increasing the length of the CNT.

CONCLUSION

Modern first-principle calculations aim at bringing computational activities up to the level where they can significantly impact innovations in electronic nanomaterial and device research. Nanostructures with many atoms and electrons can be treated only by addressing the efficiency and scalability of the algorithms on modern computing platforms with multiple hierarchical levels of parallelism. These goals can be achieved using an efficient

TABLE 4 NESSIE's main parameters and simulation results obtained using the all-electron/DFT/TDDFT/ALDA framework applied to increasingly longer (3,3)-CNTs.

SIMULATION COMPONENTS	SIMULATION DATA	5-CNT	10-CNT	20-CNT	40-CNT
System	Length (nm)	1.26	2.49	4.99	9.99
	Number of atoms	78	138	258	498
	Number of electrons	408	768	1,488	2,928
Mesh	Size muffin	2,065	2,065	2,065	2,065
	Size interstitial	149,499	126,431	233,696	446,559
	Size total	302,925	397,877	741,182	142,6125
DFT	E_t (eV)	−267.73	−268.05	−268.07	−268.28
	E_{HOMO} (eV)	−4.996	−4.823	−5	−4.955
	E_{tot} (eV)	−67,713	−128,825	−251,351	−496,359
RT-CN	Δ_t (fs)	0.01	0.01	0.01	0.01
	Total T (fs)	15	30	45	65
	Number of time steps	1,500	3,000	4,500	6,500
TDDFT	E_p (eV)	1.62	1.24	0.82	0.525
	f_p (THz)	394.13	299.83	198.27	126.94
	v_p (10^6 m/s)	0.98	1.49	1.98	2.54

The real-space mesh uses a P2-FEM discretization, while the real-time approach uses a CN (RT-CN) propagation scheme. The simulations were executed on XSEDE-Comet [126].

modeling framework that can perform real-space DFT ground-state calculations and real-time TDDFT excited-state calculations. The latter can be used to study various relevant quantum many-body effects (such as plasmonic effects) by performing electronic spectroscopy.

Spectroscopic techniques are among the most fundamental probes of matter: incoming radiation perturbs the sample, and the response to this perturbation is measured. The system is inherently excited in this process, and, hence, a calculation of ground-state properties is insufficient to interpret the response of the system. TDDFT has had considerable success modeling the interaction of electromagnetic fields with matter and obtaining spectroscopic information with absorption and emission spectra.

The article discussed the NESSIE software, which has been fundamentally designed to take advantage of parallel optimization at various levels of the entire modeling process. NESSIE benefits from the linear scaling capabilities of real-space mesh techniques and DD methods to perform all-electron (full-core potential) calculations. The modeling approach is tailored to optimally take advantage of the full capability of the state-of-the-art FEAST eigensolver, which can achieve significant parallel scalability on modern HPC architectures. With the success in meeting these challenges, NESSIE is currently able to extend the first-principle simulations to very large atomistic structures (i.e., many thousands of electrons at the level of all-electron/DFT/TDDFT/ALDA theory).

The modeling framework opens new perspectives for addressing the numerical challenges in TDDFT excited-state calculations to operate the full range of electronic spectroscopy and study the nanoscopic many-body effects in arbitrary complex molecules and finite-size, large-scale nanostructures. It is expected that the NESSIE software and associated numerical components can become a new valuable new tool for the scientific community to investigate the fundamental electronic properties of numerous nanostructured materials.

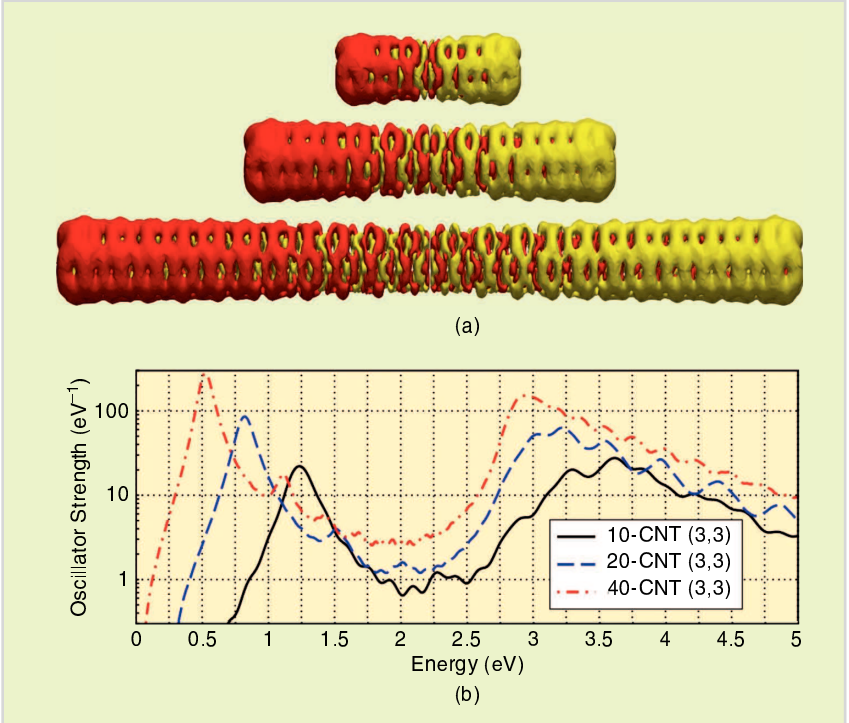

FIGURE 8 The (a) 4D isosurface plots and (b) computed absorption spectra for three (3,3)-CNTs presented in Table 4 (10, 20, and 40 unit cells). The selected energy range outlines the lowest excitation peak, which keeps shifting left (red shift) with longer nanostructures. The corresponding 4D isosurface plots of the response electron density provide visual information about the dynamic of these plasmonic excitations.

ACKNOWLEDGMENTS

This work was supported by the National Science Foundation under grants CCF-1510010 and SI2-SSE 1739423. The CNT calculations used the Extreme Science and Engineering Discovery Environment, which is supported by National Science Foundation (grant ACI-1548562).

ABOUT THE AUTHORS

James Kestyn (jamkes78@gmail.com) is with Stellar Science Ltd Co., Albuquerque, New Mexico.

Eric Polizzi (epolizzi@engin.umass.edu) is with the Department of Electrical and Computer Engineering and the Department of Mathematics and Statistics, University of Massachusetts, Amherst.

REFERENCES

[1] R. M. Martin, *Electronic Structure: Basic Theory and Practical Methods*. Cambridge, U.K.: Cambridge Univ. Press, 2004.

[2] J. Kohanoff, *Electronic Structure Calculations for Solids and Molecules: Theory and Computational Methods*. Cambridge, U.K.: Cambridge Univ. Press, 2006.

[3] P. Hohenberg and W. Kohn, "Inhomogeneous electron gas," *Phys. Rev.*, vol. 136, no. 3B, pp. B864–B871, 1964. doi: 10.1103/PhysRev.136.B864.

[4] W. Kohn and L. J. Sham, "Self-consistent equations including exchange and correlation effects," *Phys. Rev.*, vol. 140, no. 4A, pp. A1133–A1138, 1965. doi: 10.1103/PhysRev.140.A1133.

[5] K. Burke, "Perspective on density functional theory," *J. Chem. Phys.*, vol. 136, no. 15, p. 150,901, 2012. doi: 10.1063/1.4704546.

[6] L. J. Sham, "Theoretical and computational development Some efforts beyond the local density approximation," *Int. J. Quantum Chem.*, vol. 56, no. 4, pp. 345–350, 2004. doi: 10.1002/qua.560560420.

[7] V. I. Anisimov, *Strong Coulomb Correlations in Electronic Structure Calculations: Beyond the Local Density Approximation*. Gordon and Breach Science Publisher, 2000.

[8] E. M. Stoudenmire, L. O. Wagner, S. R. White, and K. Burke, "One-dimensional continuum electronic structure with the density matrix renormalization group and its implications for density functional theory," *Phys. Rev. Lett.*, vol. 109, no. 5, p. 056402, 2012. doi: 10.1103/PhysRevLett.109.056402.

[9] W. G. Aulbur, L. Jönsson, and J. W. Wilkins, "Quasiparticle calculations in solids," *Solid State Phys.*, vol. 54, pp. 1–218, 2000.

[10] C. A. Ullrich, *Time-Dependent Density-Functional Theory: Concepts and Applications*. London: Oxford Univ. Press, 2012.

[11] M. A. L. Marques, N. T. Maitra, F. M. S. Nogueira, E. K. U. Gross, and A. Rubio, *Fundamentals of Time-Dependent Density Functional Theory* (Lecture Notes in Physics), vol. 837. Berlin: Springer-Verlag, 2012.

[12] G. Onida, L. Reining, and A. Rubio, "Electronic excitations: Density-functional versus many-body Green's-function approaches," *Rev. Mod. Phys.*, vol. 74, no. 2, pp. 601–658, 2002. doi: 10.1103/RevModPhys.74.601.

[13] E. Runge and E. K. U. Gross, "Density-functional theory for time-dependent systems," *Phys. Rev. Let*, vol. 52, no. 12, pp. 997–1000, 1984. doi: 10.1103/PhysRevLett.52.997.

[14] K. Burke, J. Werschnik, and E. K. U. Gross, "Time-dependent density functional theory: Past, present, and future," *J. Chem. Phys.*, vol. 123, no. 6, p. 062206, 2005. doi: 10.1063/1.1904586.

[15] K. Yabana and G. F. Bertsch, "Application of the time-dependent local density approximation to optical activity," *Phys. Rev. A*, vol. 60, no. 2, p. 1271, 1999. doi: 10.1103/PhysRevA.60.1271.

[16] K. Yabana, T. Nakatsukasa, J.-I. Iwata, and G. F. Bertsch, "Real-time, real-space implementation of the linear response time-dependent density-functional theory," *Phys. Stat. Sol. (b)*, vol. 243, no. 5, pp. 1121–1138, 2006. doi: 10.1002/pssb.200642005.

[17] X. Andrade et al., "Time-dependent density-functional theory in massively parallel computer architectures: The octopus project," *J. Phys., Cond. Matt.*, vol. 24, no. 23, p. 233,202, 2012. doi: 10.1088/0953-8984/24/23/233202.

[18] *Octopus*. (2020). Accessed: Mar. 2020. [Online]. Available: http://www.tddft.org/programs/octopus/

[19] NWChem. Accessed: Mar. 2020. [Online]. Available: http://www.nwchem-sw.org/index.php/Main_Page

[20] GPAW. [Online]. Available: https://wiki.fysik.dtu.dk/gpaw/

[21] M. E. Casida, "Time-dependent density-functional response theory for molecules," in *Recent Advances in Density Functional Methods, Part I*, D. P. Chong, Ed. Singapore: World Scientific, 1995, p. 155.

[22] E. Lorin de la Grandmaison, S. B. Gowda, Y. Saad, M. L. Tiago, and J. R. Chelikowsky, "Efficient computation of the coupling matrix in time-dependent density functional theory," *Comput. Phys. Commun.*, vol. 167, no. 1, pp. 7–22, 2005. doi: 10.1016/j.cpc.2004.12.003.

[23] W. R. Burdick, Y. Saad, L. Kronik, M. Jain, and J. Chelikowsky, "Parallel implementations of time-dependent density functional theory," *Comput. Phys. Commun.*, vol. 156, no. 1, pp. 22–42, 2003. doi: 10.1016/S0010-4655(03)00413-2.

[24] S. Meng and E. Kaxiras, "Real-time, local basis-set implementation of time-dependent density functional theory for excited state dynamics simulations," *J. Chem. Phys.*, vol. 129, no. 5, p. 054110, 2008. doi: 10.1063/1.2960628.

[25] T. Beck, "Real-space mesh techniques in density-functional theory," *Rev. Modern Phys.*, vol. 72, no. 4, p. 1041, 2000. doi: 10.1103/RevModPhys.72.1041.

[26] P. F. Batcho, "Computational method for general multicenter electronic structure calculations," *Phys. Rev. B*, vol. 61, no. 6, p. 7169, 2000. doi: 10.1103/PhysRevE.61.7169.

[27] S. R. White, J. W. Wilkins, and M. P. Teter, "Finite element method for electronic structure," *Phys. Rev. B*, vol. 39, no. 9, p. 5819, 1989. doi: 10.1103/PhysRevB.39.5819.

[28] J. R. Chelikowsky, N. Troullier, and Y. Saad, "Finite-difference-pseudopotential method: Electronic structure calculations without a basis," *Phys. Rev. Lett.*, vol. 72, no. 8, p. 1240, 1994. doi: 10.1103/PhysRevLett.72.1240.

[29] E. Tsuchida and M. Tsukada, "Electronic-structure calculations based on finite-element method," *Phys. Rev. B*, vol. 52, no. 8, p. 5573, 1995. doi: 10.1103/PhysRevB.52.5573.

[30] N. A. Modine, G. Zumbach, and E. Kaxiras, "Adaptive-coordinate real-space electronic structure calculations for atoms, molecules, and solids," *Phys. Rev. B*, vol. 55, no. 16, p. 10,289, 1997. doi: 10.1103/PhysRevB.55.10289.

[31] E. L. Briggs, D. J. Sullivan, and J. Bernholc, "Real-space multigrid-based approach to large-scale electronic structure calculations," *Phys. Rev. B*, vol. 54, no. 20, p. 14,362, 1996. doi: 10.1103/PhysRevB.54.14362.

[32] M. Heisakanen, T. Torsti, M. J. Puska, and R. M. Nieminen, "Multigrid method for electronic structure calculations," *Phys. Rev. B*, vol. 63, no. 24, p. 245,106, 2001. doi: 10.1103/PhysRevB.63.245106.

[33] S. Goedecker, "Linear scaling electronic structure methods," *Rev. Modern Phys.*, vol. 71, no. 4, p. 1085, 1999. doi: 10.1103/RevModPhys.71.1085.

[34] J. E. Pask, B. M. Klein, P. A. Sterne, and C. Y. Fong, "Finite-element methods in electronic structure theory," *Comput. Phys. Commun.*, vol. 135, no. 1, pp. 1–34, 2001. doi: 10.1016/S0010-4655(00)00212-5.

[35] J. R. Chelikowsky, "The pseudopotential-density functional method applied to nanostructures," *J. Phys. D*, vol. 33, no. 8, p. R33, 2000. doi: 10.1088/0022-3727/33/8/201.

[36] T. Torsti et al., "Three real-space discretization techniques in electronic structure calculations," *Physica Status Solidi (b)*, vol. 243, no. 5, pp. 1016–1053, 2006. doi: 10.1002/pssb.200541348.

[37] L. Lehtovaara, V. Havu, and M. Puska, "All-electron density functional theory and time-dependent density functional theory with high-order finite elements," *J. Chem. Phys.*, vol. 131, no. 5, p. 054103, 2009. doi: 10.1063/1.3176508.

[38] S. Baroni and P. Giannozzi, "Towards very large scale electronic structure calculations," *Europhys. Lett.*, vol. 17, no. 6, p. 547, 1992. doi: 10.1209/0295-5075/17/6/012.

[39] L. Lin, C. Yang, J. C. Meza, J. Lu, L. Ying, and W. E, "SelInv: An algorithm for selected inversion of a sparse symmetric," *Matrix ACM Trans. Math. Softw.*, vol. 37, no. 4, pp. 1–19, 2011. doi: 10.1145/1916461.1916464.

[40] D. Zhang and E. Polizzi, "Linear scaling techniques for first-principle calculations of large nanowire devices," in *Proc. 2008 NSTI Nanotechnol. Conf. Trade Show*, vol. 1, pp. 12–15.

[41] G. Golub and H. A. van der Vorst, "Eigenvalue computation in the 20th century," *J. Comput. Appl. Math.*, vol. 123, nos. 1–2, pp. 35–65, 2000. doi: 10.1016/S0377-0427(00)00413-1.

[42] Z. Bai, J. Demmel, J. Dongarra, A. Ruhe, and H. van der Vorst, *Templates for the solution of Algebraic Eigenvalue Problems: A Practical Guide*. Philadelphia: Society for Industrial and Applied Mathematics, 2000.

[43] "Freely available software for linear algebra (September 2018)." Netlib Repository. [Online]. Available:http://www.netlib.org/utk/people/JackDongarra/la-sw.html

[44] T. Sakurai and H. Sugiura, "A projection method for generalized eigenvalue problems using numerical integration," *J. Comput. Appl. Math.*, vol. 159, no. 1, pp. 119–128, 2003. doi: 10.1016/S0377-0427(03)00565-X.

[45] T. Sakurai and H. Tadano, "CIRR: A Rayleigh-Ritz type method with contour integral for generalized eigenvalue problems," *Hokkaido Math. J.*, vol. 36, no. 4, pp. 745–757, 2007. doi: 10.14492/hokmj/1272848031.

[46] A. Imakura, L. Du, and T. Sakurai, "A block Arnoldi-type contour integral spectral projection method for solving generalized eigenvalue problems," *Appl. Math. Lett.*, vol. 32, pp. 22–27, June 2014. doi: 10.1016/j.aml.2014.02.007.

[47] A. P. Austin and L. N. Trefethen, "Computing eigenvalues of real symmetric matrices with rational filters in real arithmetic," *SIAM J. Sci. Comput.*, vol. 37, no. 3, pp. A1365–A1387, 2015. doi: 10.1137/140984129.

[48] E. Polizzi, "Density-matrix-based algorithm for solving eigenvalue problems," *Phys. Rev. B*, vol. 79, no. 11, p. 115,112, 2009. doi: 10.1103/PhysRevB.79.115112.

[49] The FEAST Eigenvalue Solver. [Online]. Available: http://www.feast-solver.org

[50] P. Tang and E. Polizzi, "FEAST as a subspace iteration eigensolver accelerated by approximate spectral projection," *SIAM J. Matrix Anal. Appl.*, vol. 35, no. 2, pp. 354–390, 2014. doi: 10.1137/13090866X.

[51] S. Güttel, E. Polizzi, P. T. Tang, and G. Viaud, "Optimized quadrature rules and load balancing for the FEAST eigenvalue solver," *SIAM J. Sci. Comput.*, vol. 37, no. 4, pp. 2100–2122, 2015. doi: 10.1137/140980090.

[52] NESSIE Software. Accessed: June 2020. [Online]. Available: http://www.nessie-code.org

[53] E. Polizzi and N. Ben Abdallah, "Self-consistent three-dimensional models for quantum ballistic transport in open systems," *Phys. Rev. B*, vol. 66, no. 24, p. 245,301, 2002. doi: 10.1103/PhysRevB.66.245301.

[54] J. C. Slater, "Wave functions in a periodic potential," *Phys. Rev.*, vol. 51, no. 10, pp. 846–851, 1937. doi: 10.1103/PhysRev.51.846.

[55] H. Si, "TetGen, a Delaunay-based quality tetrahedral mesh generator," *ACM Trans. Math. Softw.*, vol. 41, no. 2, pp. 1–36, 2015. doi: 10.1145/2629697.

[56] H. Si. TetGen. (2020). Accessed: Mar. 2020. [Online]. Available: http://wias-berlin.de/software/index.jsp?id=TetGen&lang=1

[57] B. N. Harmon and D. D. Koelling, "Technique for rapid solution of the APW secular equation," *J. Phys. C, Solid-State Phys.*, vol. 7, no. 11, p. 210, 1974.

[58] E. Sjöstedt and L. Nordström, "Efficient solution of the non-linear augmented plane wave secular equation," *J. Phys., Condens. Matter*, vol. 14, pp. 12,485–12,494, Nov. 2002.

[59] W.-J. Beyn, "An integral method for solving nonlinear eigenvalue problems," *Linear Algebra Appl.*, vol. 436, no. 10, pp. 3839–3863, 2012. doi: 10.1016/j.laa.2011.03.030.

[60] B. Gavin, A. Miedlar, and E. Polizzi, "FEAST eigensolver for nonlinear eigenvalue problems," *J. Comput. Sci.*, vol. 27, pp. 107–117, July 2018. doi: 10.1016/j.jocs.2018.05.006.

[61] O. K. Andersen, "Linear methods in band theory," *Phys. Rev. B*, vol. 12, no. 8, pp. 3060–3083, 1975. doi: 10.1103/PhysRevB.12.3060.

[62] D. J. Singh, "Ground-state properties of lanthanum: Treatment of extend-core states," *Phys. Rev. B*, vol. 43, no. 8, p. 6388, 1991. doi: 10.1103/PhysRevB.43.6388.

[63] E. Sjöstedt, L. Nordström, and D. J. Singh, "An alternative way of linearizing the augmented plane-wave method," *Solid State Commun.*, vol. 114, no. 1, pp. 15–20, 2000. doi: 10.1016/S0038-1098(99)00577-3.

[64] G. K. H. Madsen, P. Blaha, K. Schwarz, E. Sjöstedt, and L. Nordström, "Efficient linearization of the augmented plane-wave method," *Phys. Rev. B*, vol. 64, no. 19, p. 195,134, 2001. doi: 10.1103/PhysRevB.64.195134.

[65] D. J. Singh and L. Nordstrom, *Planewaves, Pseudopotentials, and the LAPW Method*, 2nd ed. New York: Springer-Verlag, 2006.

[66] H. Hellmann, "A new approximation method in the problem of many electrons," *J. Chem. Phys.*, vol. 3, no. 1, p. 61, 1935. doi: 10.1063/1.1749559.

[67] J. C. Phillips and L. Kleinman, "New method for calculating wave functions in crystals and molecules," *Phys. Rev.*, vol. 116, no. 2, p. 287, 1959. doi: 10.1103/PhysRev.116.287.

[68] L. Kleinman and D. M. Bylander, "Efficacious form for model pseudopotentials," *Phys. Rev. Lett.*, vol. 48, no. 20, p. 1425, 1982. doi: 10.1103/PhysRevLett.48.1425.

[69] P. E. Blöchl, "Projector augmented-wave method," *Phys. Rev. B*, vol. 50, no. 24, p. 17,953, 1994. doi: 10.1103/PhysRevB.50.17953.

[70] A. Levin, D. Zhang, and E. Polizzi, "FEAST fundamental framework for electronic structure calculations: Reformulation and solution of the muffin-tin problem," *Comput. Phys. Commun.*, vol. 183, no. 11, pp. 2370–2375, 2012. doi: 10.1016/j.cpc.2012.06.004.

[71] J. Kestyn, "Parallel algorithms for time dependent density functional theory in real-space and real-time," Ph.D. dissertation, Depart. Elect. Comput. Eng., Univ. Massachusetts Amherst, 2018.

[72] J. Kestyn, E. Polizzi, and P. T. Tang, "FEAST eigensolver for non-Hermitian problems," *SIAM J. Sci. Comput.*, vol. 38, no. 5, pp. S772–S799, 2016. doi: 10.1137/15M1026572.

[73] D. G. Anderson, "Iterative procedures for nonlinear integral equations," *J. ACM*, vol. 12, no. 4, pp. 547–560, 1965. doi: 10.1145/321296.321305.

[74] C. G. Broyden, "A class of methods for solving nonlinear simultaneous equations," *Math. Comput.*, vol. 19, no. 92, pp. 577–593, 1965. doi: 10.1090/S0025-5718-1965-0198670-6.

[75] P. Pulay, "Convergence acceleration of iterative sequences. the case of SCF iteration," *Chem. Phys. Lett.*, vol. 73, no. 2, pp. 393–398, 1980. doi: 10.1016/0009-2614(80)80396-4.

[76] P. Pulay, "Improved SCF convergence acceleration," *J. Comput. Chem.*, vol. 3, no. 4, pp. 556–560, 1982. doi: 10.1002/jcc.540030413.

[77] K. N. Kudin, G. E. Scuseria, and E. Cances, "A black-box self-consistent field convergence algorithm: One step closer," *J. Chem. Phys.*, vol. 116, no. 19, pp. 8255–8261, 2002. doi: 10.1063/1.1470195.

[78] C. Yang, W. Gao, and J. C. Meza, "On the convergence of the self-consistent field iteration for a class of non-linear eigenvalue problems," *SIAM J. Matrix Anal. Appl.*, vol. 30, no. 4, pp. 1773–1788, 2009. doi: 10.1137/080716293.

[79] H. F. Walker and P. Ni, "Anderson acceleration for fixed-point iterations," *SIAM J. Numer. Anal.*, vol. 49, no. 4, pp. 1715–1735, 2011. doi: 10.1137/10078356X.

[80] B. Gavin and E. Polizzi, "Non-linear eigensolver-based alternative to traditional SCF methods," *J. Chem. Phys.*, vol. 138, no. 19, p. 194,101, 2013. doi: 10.1063/1.4804419.

[81] V. Eyert, "A comparative study on methods for convergent acceleration of iterative vector sequences," *Comput. Phys.*, vol. 124, no. 2, pp. 271–285, 1996. doi: 10.1006/jcph.1996.0059.

[82] Y. Saad and M. H. Schultz, "GMRES: A generalized minimal residual algorithm for solving nonsymmetric linear systems," *SIAM J. Sci. Statist. Comput.*, vol. 7, no. 3, pp. 856–869, 1986. doi: 10.1137/0907058.

[83] Y. Saad, J. R. Chelikowsky, and S. M. Shontz, "Numerical methods for electronic structure calculations of materials," *SIAM Rev.*, vol. 52, no. 1, pp. 3–54, 2010. doi: 10.1137/060651653.

[84] *FHI-aims*. (2020). Accessed: Mar. 2020. [Online]. Available: https://aimsclub.fhi-berlin.mpg.de/

[85] J. P. Perdew and A. Zunger, "Self-interaction correction to density- functional approximations for many-electron systems," *Phys. Rev. B*, vol. 23, no. 10, p. 5048, 1981. doi: 10.1103/PhysRevB.23.5048.

[86] J. Kestyn, V. Kalantzis, E. Polizzi, and Y. Saad, "PFEAST: A high performance eigenvalue solver using distributed-memory linear solvers," in *Proc Int. Conf. High Perform Comput. Network., Storage Anal.*, 2016, vol. 2016, no. 16, pp. 178–189. doi: 10.1109/SC.2016.15.

[87] *Math Kernel Library*. (2020). Intel. Accessed: Mar. 2020. [Online]. Available: http://software.intel.com/en-us/intel-mkl

[88] P. R. Amestoy, I. S. Duff, J. L'Excellent, and J. Koster, "MUMPS: A general purpose distributed memory sparse solver," in *Applied Parallel Computing. New Paradigms for HPC in Industry and Academia*, T. Sørevik, F. Manne, A. H. Gebremedhin, and R. Moe, Eds. New York: Springer-Verlag, 2000, pp. 121–130.

[89] A. Castro, M. A. L. Miguel, and A. Rubio, "Propagators for the time-dependent Kohn-Sham equations," *J. Chem. Phys.*, vol. 121, no. 8, pp. 3425–3433, 2004. doi: 10.1063/1.1774980.

[90] J. Crank and P. Nicolson, "A practical method for numerical evaluation of solutions of partial differential equations of the heat conduction type," *Proc. Camb. Phil. Soc.*, vol. 43, no. 1, pp. 50–67, 1947. doi: 10.1017/S0305004100023197.

[91] T. Y. Mikhailova and V. I. Pupyshev, "Symmetric approximations for the evolution operator," *Phys. Lett. A*, vol. 257, nos. 1–2, pp. 1–16, 1999. doi: 10.1016/S0375-9601(99)00242-X.

[92] W. Magnus, "On the exponential solutions of differential equations for a linear operator," *Commun. Pure Appl. Math.*, vol. VII, no. 1954, pp. 649–673, 1954.

[93] Z. Chen and E. Polizzi, "Spectral-based propagation schemes for time-dependent quantum systems with application to carbon nanotubes," *Phys. Rev. B*, vol. 82, no. 20, p. 205,410, 2010. doi: 10.1103/PhysRevB.82.205410.

[94] A. Russakoff, Y. Li, S. He, and K. Varga, "Accuracy and computational efficiency of real-time subspace propagation schemes for the time-dependent density functional theory," *J. Chem. Phys.*, vol. 144, no. 20, p. 204,125, 2016. doi: 10.1063/1.4952646.

[95] X. Andrade, S. Botti, M. A. L. Marques, and A. Rubio, "Time-dependent density functional theory scheme for efficient calculations of dynamic (hyper)polarizabilities," *J. Chem. Phys.*, vol. 126, no. 18, p. 184,106, 2007. doi: 10.1063/1.2733666.

[96] Y. Takimoto, "A real-time time-dependent density functional theory method for calculating linear and nonlinear dynamic optical response," Ph.D. thesis, Univ. of Washington, 2008.

[97] V. Astapenko, *Interaction of Ultrashort Electromagnetic Pulses with Matter*. New York: Springer-Verlag, 2013.

[98] R. C. Hilborn, "Einstein coefficients, cross sections, f values, dipole moments, and all that," *Amer. J. Phys.*, vol. 50, no. 11, pp. 982–986, 1982. doi: 10.1119/1.12937.

[99] Z. Chen, "Computational All-electron time-dependent density functional theory in real-space and real-time: Applications to molecules and nanostructures," Doctoral Dissertations, UMass Amherst, 2013.

[100] E. Polizzi and S. Yngvesson, "Universal nature of collective plasmonic excitations in finite 1-D carbon-based nanostructures," *Nanotechnology*, vol. 26, no. 32, p. 325,201, 2015. doi: 10.1088/0957-4484/26/32/325201.

[101] T. E. Sharp, "Potential-energy curves for molecular hydrogen and its ions," *Atomic Data Nucl. Data Tables*, vol. 2, pp. 119–169, Dec. 1970. doi: 10.1016/S0092-640X(70)80007-9.

[102] G. Herzberg, *Molecular Spectra and Molecular Structure. Vol. 1: Spectra of Diatomic Molecules*, 2nd ed. New York: Van Nostrand Reinhold, 1950.

[103] O. W. Richardson, *Molecular Hydrogen and its Spectrum*, vol. 23. New Haven, CT: Yale Univ. Press, 1934.

[104] C. Backx, G. R. Wight, and M. J. Van der Wiel, "Oscillator strengths (10-70 ev) for absorption, ionization and dissociation in H_2, Hd and D_2, obtained by an electron-ion coincidence method," *J. Phys. B, At. Mol. Opt. Phys.*, vol. 9, no. 2, p. 315, 1976. doi: 10.1088/0022-3700/9/2/018.

[105] W. F. Chan, G. Cooper, and C. E. Brion, "Absolute optical oscillator strengths for discrete and continuum photoabsorption of carbon monoxide (7–200 ev) and transition moments for the x 1σ+ a 1π system," *Chem. Phys.*, vol. 170, no. 1, pp. 123–138, 1993. doi: 10.1016/0301-0104(93)80098-T.

[106] C.-Y. Chung, E. P. Chew, B.-M. Cheng, M. Bahou, and Y.-P. Lee, "Temperature dependence of absorption cross-section of H_2O, HOD, and D_2O in the spectral region 140-193 nm," *Nucl. Instrum. Methods Phys. Res. A, Accelerators, Spectr., Detect. Assoc. Equip.*, vol. 467-468, pp. 1572–1576, July 2001. doi: 10.1016/S0168-9002(01)00762-8.

[107] B.-M. Cheng et al., "Quantitative spectroscopic and theoretical study of the optical absorption spectra of H_2O, HOD, and D_2O in the 125-145 nm region," *J. Chem. Phys.*, vol. 120, no. 1, pp. 224–229, 2004. doi: 10.1063/1.1630304.

[108] D. H. Katayama, R. E. Huffman, and C. L. O'Bryan, "Absorption and photoioniza- tion cross sections for H2O and D2O in the vacuum ultraviolet," *J. Chem. Phys.*, vol. 59, no. 8, pp. 4309–4319, 1973. doi: 10.1063/1.1680627.

[109] W. F. Chan, G. Cooper, and C. E. Brion, "The electronic spectrum of water in the discrete and continuum regions. absolute optical oscillator strengths for photoabsorption (6-200 eV)," *Chem. Phys.*, vol. 178, nos. 1–3, pp. 387–400, 1993. doi: 10.1016/0301-0104(93)85078-M.

[110] F. Z. Chen and C. Y. R. Wu, "Temperature-dependent photoabsorption cross sections in the VUV-UV region. I. Methane and ethane," *J. Quant. Spectrosc. Radiat. Transf.*, vol. 85, no. 2, pp. 195–209, 2004. doi: 10.1016/S0022-4073(03)00225-5.

[111] K. Kameta, N. Kouchi, M. Ukai, and Y. Hatano, "Photoabsorption, photoionization, and neutral-dissociation cross sections of simple hydrocarbons in the vacuum ultraviolet range," *J. Electron Spectrosc. Related Phenomena*, vol. 123, nos. 2–3, pp. 225–238, 2002. doi: 10.1016/S0368-2048(02)00022-1.

[112] G. Cooper, G. R. Burton, W. F. Chan, and C. E. Brion, "Absolute oscillator strengths for the photoabsorption of silane in the valence and Si 2p and 2s regions (7.5-350 ev)," *Chem. Phys.*, vol. 196, nos. 1–2, pp. 293–306, 1995. doi: 10.1016/0301-0104(95)00085-3.

[113] A. Dawes, N. Pascual, S. V. Hoffmann, N. C. Jones, and N. J. Mason, "Vacuum ultraviolet photoabsorption spectroscopy of crystalline and amorphous benzene," *Phys. Chem. Chem. Phys.*, vol. 19, no. 40, pp. 27,544–27,555, 2017. doi: 10.1039/C7CP05319C.

[114] E. E. Rennie, C. A. F. Johnson, J. E. Parker, D. M. P. Holland, D. A. Shaw, and M. A. Hayes, "A photoabsorption, photodissociation and photoelectron spectroscopy study of C6H6 and C6D6," *Chem. Phys.*, vol. 229, no. 1, pp. 107–123, 1998. doi: 10.1016/S0301-0104(97)00373-X.

[115] K. Lopata and N. Govind, "Modeling fast electron dynamics with real-time time-dependent density functional theory: Application to small molecules and chromophores," *J. Chem. Theory Comput.*, vol. 7, no. 5, pp. 1344–1355, 2011. doi: 10.1021/ct200137z.

[116] M. I. Stockman, "Nanoplasmonics: The physics behind the applications," *Phys. Today*, vol. 64, no. 2, pp. 39–44, 2011. doi: 10.1063/1.3554315.

[117] N. J. Halas, "Connecting the dots: Reinventing optics for nanoscale dimensions," *Proc. Natl. Acad. Sci.*, vol. 106, no. 10, pp. 3463–3644, 2009.

[118] L. Novotny and N. van Hulst, "Antennas for light," *Nature Photon.*, vol. 5, no. 2, p. 83, 2011. doi: 10.1038/nphoton.2010.237.

[119] H. Cang et al., "Probing the electromagnetic field of a 15 nanometre hotspot by single molecule imaging," *Nature*, vol. 469, no. 7330, p. 385, 2011. doi: 10.1038/nature09698.

[120] J. B. Khurgin, "How to deal with the loss in plasmonics and metamaterials," *Nature Nanotechnol.*, vol. 10, no. 1, pp. 2–6, 2015. doi: 10.1038/nnano.2014.310.

[121] C. Kittel, *Introduction to Solid State Physics*, 8th ed. Hoboken, NJ: Wiley, 2005.

[122] S. Tomonaga, "Remarks on Bloch's method of sound waves applied to many-fermion problems," *Prog. Theor. Phys.*, vol. 5, no. 4, pp. 544–569, 1950. doi: 10.1143/ptp/5.4.544.

[123] J. Luttinger, "An exactly soluble model of a many-fermion system," *J. Math. Phys.*, vol. 4, no. 9, pp. 1154–1162, 1963. doi: 10.1063/1.1704046.

[124] V. K. Deshpande, M. Bockrath, L. Glazman, and A. Yacoby A, "Electron liquids and solids in one dimension," *Nature*, vol. 464, no. 7286, p. 209, 2010. doi: 10.1038/nature08918.

[125] C. Kane, L. Balents, and P. A. Fisher, "Coulomb interactions and mesoscopic effects in carbon nanotubes," *Phys. Rev. Lett.*, vol. 79, no. 25, p. 5086, 1997. doi: 10.1103/physrevlett.79.5086.

[126] J. Towns et al., "XSEDE: Accelerating scientific discovery," *Comput. Sci. Eng.*, vol. 16, no. 5, pp. 62–74, Sept./Oct. 2014. doi: 10.1109/MCSE.2014.80.z